SCIENTIFIC CULTURE

www.sci-cult.com

SCIENTIFIC CULTURE, Vol. 12, No. 2.1, (2026), pp. 4666-4678
Open Access. Online & Print

DOI: 10.5281/zenodo.122126359

A SCRUTINY-AUGMENTED CONVOLUTION U-NET MODEL FOR CAROTID PLAQUE SEGMENTATION

Prathiba Jonnala[1*] and G. Sitaramanjaneya Reddy[2]

[1,2]Vignan's Foundation for Science, Technology and Research (Deemed to be University), Vadlamudi, Andhra Pradesh, India, jp_ece@vignan.ac.in

Received: 01/02/2026
Accepted: 05/03/2026

Corresponding Author: Prathiba Jonnala (jp_ece@vignan.ac.in)

ABSTRACT

Strokes rank higher than most other causes of death. Although segmenting carotid artery atherosclerotic plaques from ultrasound images have enormous benefits in both avoiding and managing ischemic stroke. However, it is still difficult due to the hazy plaque boundaries and significant ultrasonic noise. Deep network context information can be gathered through scrutiny models, and current self-scrutiny techniques in particular have demonstrated to be useful for image segmentation tasks. The most recent test-augmented convolution models aim to capture long-range interactions by combining convolution and self-test feature maps. In order to increase the amount of spatial synthesis, this study suggests SAC-U-Net (supervision augmented convolution U-Net) that incorporates supervision augmented computation into the bottleneck of the encoder-decoder segmentation design. The advanced convolution encoder-decoder architecture was developed as an unsupervised learning strategy for conditioning the variables of U-Net by amount of unlabeled data in order to address the issue of a shortage of labelled examples. The advanced convolution encoder-decoder network's learnt parameters were then used to start a U-Net from the tagged images for fine-tuning. SAC-U-Net Model significantly outperforms other cutting-edge techniques in the lesion segmentation challenge, demonstrating the usefulness and strong explanatory power of the suggested approach.

KEYWORDS: Stroke, Carotid Plaque Segmentation, Scrutiny-Augmented Convolution U-Net, Ultrasound Images, and Deep Convolution Encoder–Decoder Network.

1. INTRODUCTION

Internal carotid artery (ICA) atherosclerotic plaques are the main contributor to cardiovascular illnesses, which have a significant death and morbidity rate worldwide [1]. Studies have demonstrated that carotid plaque is an accurate marker of atherosclerosis [3]. Several medical imaging methods can be used to examine carotid plaques, including CT (computed tomography), MRI (magnetic resonance imaging), X-ray, and US (ultrasonography). Ultrasonography is favoured above the others due to its portability, low cost, lack of radiation, convenience of use, and non-invasiveness [4,5,6]. The recorded carotid artery ultrasound images contain a variety of data, including carotid intima-media width, plaque sizes, locations, echo intensities, plaque surface morphologies, etc. The image data displays the diseased status as well as the condition of the arteries in the heart and brain. As a result, precise carotid plaque segmentation is crucial for later diagnosis, assessment, and prognosis. Despite this, carotid plaques frequently adhere to blood vessel boundaries, and the forms of plaque are complicated, making manual segmentation challenging. Echo errors and speckle noise reduce the clarity of ultrasound images. Additionally, segmentation accuracies are based on subjective evaluations of sonographers. The normal shortage of qualified and experienced sonographers still exists.

As a result, numerous research investigations on computerized plaque carotid segmentation have been conducted. Reliable feature extraction skills are needed for segmentations to correctly coincide with vascular borders and patches at pixel levels. Advancements in DL (deep learning), DNNs (deep neural networks), particularly those utilising CNNs (convolution neural networks), can successfully extract high-dimensional abstract features from ultrasound images. [14]. Although these techniques have been very effective at segmenting ultrasound images of carotid plaques, there are still significant drawbacks. On the one hand, the problem of extracting features from ultrasound images with poor contrast and quality continues to be difficult for DNNs. Additionally, carotid plaques can have erratic forms and range in size. On the other hand, to build efficient and workable segmentation algorithms, huge pixel-level datasets with annotations are needed. Such requirements, however, cannot be met by the available datasets. This study introduces a novel method called SAC-U-Net, which automatically segments carotid plaque on ultrasound images using a sort of convolution networks with an encoder-decoder architecture.

The remainder of the article is outlined as follows: Section 2 lists related work. In section 3, the proposed SAC-U-Net model is presented. Section 4 presents the experimental findings. Section 5 provides the conclusion and suggestions for future development.

2. RELATED WORK

In order to develop the segmentation algorithm and produce the total plaque area (TPA) measurement, Zhou et al. [5] used a DL -based approach with a modified U-Net. In our investigation, 510 plaques from 144 sufferers were included in the total, and the data set was randomly divided into training and testing groups of 2/3 and 1/3. This was done using the MC (Monte Carlo) cross-validation methods. The Plates (510 in numbers) were personally marked by two qualified observers for ground truth indications. Two U-Net models (M1 and M2) utilising two different sets of ground truths and terrain data from two observers in order to assess accuracies, variability, and sensitivities of information sets utilised to train our approaches. However, ultrasound image noises have an impact on how gradients are initialised.

Akkus et al. [6] used representations of carotid lesions collected concurrently on BMUS (B-mode ultrasound) and CEUS (contrast-enhanced ultrasound) images. This method includes non-rigid motion estimates, vessel identifications, lumen-intima segmentations, and media-adventitia segmentations. The evaluation was carried out by comparing the test (n = 28) and instructional (n = 20 carotids) data sets with manually gathered ground truth. The experimental data set preparation resulted in overall RMSE bias (root-mean-square) remaining comparable to the inter-observer variability for lumen-intima (362 192 and 388 200 m) and media-adventitia (411 224 and 393 239 m). The proposed method fully automated carotid plaque segmentations by combining BMUS and CEUS. However, growing recognitions of plaque instead of sizes was connected to risks of ruptures.

An integrated learning-based approach was put out by Qian & Yang [7] for segmenting atherosclerosis plaques in carotid arteries of ultrasound images. The auto-context iterative framework and four alternative classification algorithms are used for executing the pixel-wise categorization, respectively. The best results are produced by suggested methodologies which combine RFs (random forests) with autologous context models. Experimental findings showed that the technique performed exactly the same as

presently employed strategies. The suggested integrated learning-based methodology was useful for calculating loads of carotid plaques. However, due to disturbances in lumen, aberrations, irregularities in lumens, and echo-lucent plaques in routine images, it may be complex and erroneous.

The initial 3D direct volume-driven level-set algorithm was developed by Cheng et al. [8] for separating plaques using 3D arterial ultrasound images. Prior to being distorted by an immediate three-dimensional in-nature limited growing level-set technique, the plate regions are initially initialised using internal and exterior wall borders produced using a semi-automatic technique, which implements axial consistency between segmented plate surfaces. This has a distinct benefit over the previously suggested slice-by-slice 2D slab segmentation approach. Previous plate boundary initialization techniques look for lines linking locations that are similar to the locations of the bed and outer wall borders. If the plate is not entirely encompassed by wall and lumen borders, this initialization method has the drawback of producing erroneous initial plate boundaries. The researchers failed to try to segment either the vascular wall or the plaque because the goal of this work was to automatically identify the common carotid artery.

A computational technique for separating atherosclerotic plaque in the carotid artery from ultrasound images was presented by Loizou et al. [9]. In order to change the original contour for the optimum match of the plaque borders, the approach first uses blood flows in images to determine original plaque contours. Leveraging 35 longitudinal ultrasound images of the carotid arteries, the method's accuracy and reproducibility were evaluated, and the findings were compared to expert manual delineations. The comparison revealed that, in most instances, no manual correction is necessary for the computerized method to produce satisfactory results. FPF (False positive fraction), FNF (false negative fraction), and TPF (true positive fraction) values of 86.44%, 84.03%, 8.5%, &and 7%, respectively. However, plaque segmentations necessitate higher levels of competences because of demarcating plaques from neighbouring walls of vessels.

On the basis of video framework standardization, scattered decrease filtration, The M-mode state-sponsored proof of identity, parametric parameters successful contours, and snake segmentation, Loizou et al.'s [11] unified approach for the differentiation of atherosclerosis plaques have been suggested and tested in the CCA ultrasonography images of carotid arteries. The heart rates in videos were first recognised, and then M-mode videos produced to show systolic and diastolic states. The parts of the images were then split into whole cardiac cycles. The algorithm is executed manually in the first frame of cardiac cycle videos, and borders of the progressing atherosclerotic plaques monitored and segmented in following frames. Two different starting techniques were used to estimate the initial bound for 20 video frames. In the initial initialization approach, the starting point of the snake contour is computed using morphological operators, and the subsequent initialization technique employs the Chan-Vese dynamic contour model. Due to distinctive picture artefacts and a lack of cellular characteristics, plaque segmentation is challenging (ten Kate et al. 2012).

Galluzzo et al. in their CAPSU publication (page 12) suggested a completely automated method for CP-S in US imaging. A new method generating procedure that automatically creates a level-based segmentation algorithm using artery wall motion analysis is fundamental to this. Constraint assessment is further utilised to enhance the starting procedure. The efficiency of CAPSU, independent of deformation analysis, was assessed and compared with traditional contouring carried out by a single ultrasound technician using ultrasound data gathered from 8 patients. The outcomes demonstrate the value of CAPSU as a precise and dependable solution for entirely computerized CPs-S in US images. The precise segmentation of artery segments in carotid arteries that have plaques present, however, presents a number of additional difficulties.

By utilizing the motion analysis of the carotid walls, Galluzzo et al. [13] provided a fully autonomous CPs segmented methodology according to the level-set with an inventive initialization procedure. Performance was evaluated using ten carotid artery US image sequences and contrasted with manual contouring performed by a skilled medical professional. Results demonstrate the method's ability to accurately segment CPs in US images without the need for user input. These techniques, however, typically call for hand-selecting anchor points, which is inaccurate and unable to handle real-time demand.

Loizou et al. [14] designed and assessed an integrated system to differentiate carotid atherosclerotic plaques using image standardisations, dispersion reduction filters, state-sponsored verifications in M-modes, active edge parameterizations, and solid separation in CCA ultrasound videos, the heart rates in videos were first

recognised, and then M modes of videos generated to ascertain systolic and diastolic conditions. The parts of the images were then split into complete cardiac cycles. Manually, the algorithm's initial few frames of the cardiac cycle videos were set, and in succeeding frames, borders of developing atherosclerotic plaques monitored and analysed. The requirement for human intervention and the widening of the lumen shape in accordance with a predetermined value, however, is these systems' principal drawback.

In a multi-center MRI research, Van Engelen et al. [15] segmented the clinically relevant carotid plaque components (fibrous/lipid tissues, calcifications, and intra-plaque haemorrhages). Voxelwise tissue classifications using standard same-center training methods were executed and compared with outcomes of two other methods that used minimal annotated same-centered data. The methods also made use of annotated data corpus belonging to several centers. This work used transfer learning techniques with same data but separate centers with various weights in evaluations with polynomial feature normalizations. Results indicated that an integration of pattern standardization and transfer learning produced the best outcomes. While significant variations in voxelwise or average volume errors were identified between the other ways and the authoritative same-center training for those approaches, the suggested methodology did not produce such discrepancies. We conclude that transfer learning and thorough feature normalization can both be helpful for the creation of supervised algorithms that work well on many kinds of datasets.

A drawback of supervised approaches is that they perform less well on data that varies from the data used for training, such as images taken with various scanners. It will be easier to implement supervised algorithms widely if fewer manual annotations are needed for each new dataset. In this work, we segment the clinically relevant carotid plaque components (fibrous/lipid tissues, calcifications, and intra-plaque haemorrhages) in the United States. Furthermore, carotid atherosclerotic plaques might range in size and form. On the other hand, massive annotated datasets at the pixel level are required to develop effective segmentation algorithms. However, the existing datasets fall short of these demands.

Due to the poor quality of ultrasonic imaging, techniques relying upon the geometrical, grayscale, which is and texture properties of the images have inadequate robustness. Furthermore, manually chosen features may not be representative because they are subjective. As a result, the categorization is not robust enough and is not precise enough.

3. PROPOSED METHODOLOGY

In order to autonomously segregate carotid plaques, this study presents SAC-U-Net, revolutionary CNNs with encoders and decoders. In order to increase the total amount of input images, additional information augmentation is employed after the images have already undergone pre-processing using AMF (Adjustable Median Filtering). This study introduced the SAC-U-Net, a ground-breaking comprehensive convolution neural network that uses encoders and decoders to autonomously detach carotid plaques. Images initially are processed using AMF and augmentations are used to enhance the total number of input images. Fig. 1 displays an outline schematic of the proposed SAC-U-Net. Our strategy outperforms other cutting-edge methods when used to train and test networks on various carotid plaque ultrasound datasets. Additional ablation trials again demonstrate the improvement of the suggested architecture.

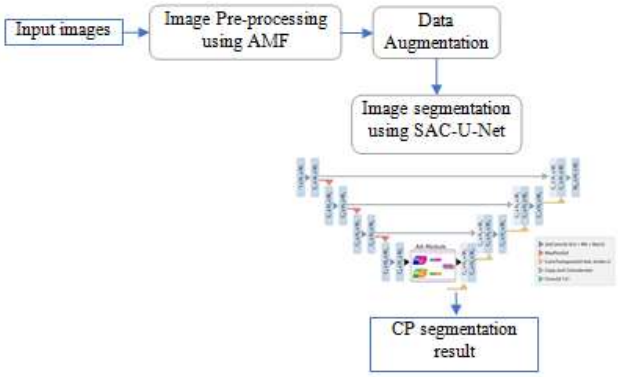

Figure 1: Block Diagram of SAC-U-Net Model for Carotid Plaque Segmentation.

Dataset Description The database contains the CCA images of 694 volunteers. This study, which adhered to the Helsinki Declaration, looked at 1,088 individuals. In all, 2,176 CCA ultrasonography pictures of the neck's left and right sides were recorded. These pictures were taken between 2003 and 2007 in the Cyprus towns of Pedoulas, Nissou, and Kambos (694 subjects, 1388 pictures). People over the age of 40 were asked to participate, and residents of three Cypriot municipalities were selected using demographic lists. Up to 2017–2018, Cypriot responders were tracked (average follow-up: 11–3 years), and any subsequent deaths or coronary heart disease were noted. A Phillips (ATL) HDI 5000

two-dimensional scanner (Seattle, WA, USA) with an L12-5 MHz bandwidth quadratic probe was used for all scans in Cyprus.

Image Pre-processing Using Adaptive Median Filtering Typically, complex noise is present in the original input image, necessitating de-noising pre-processing before image segmentation. There is a lot of interruption in the UI that was employed in this study [22]. Consequently, pre-processing an image is a necessary step. De-noising is accomplished using adaptive median filtering; the procedure is depicted in Fig. 2 and the outcomes are displayed in Fig. 3.The range that the filter focused on (x, y). covers is represented by $Range_{xy}$. It should be notedCG_{min}, CG_{max}, and CG_{mid}represent the smallest, maximum, and median values in the coverage gray area, respectively. The color gray value associated with the pixel point at (x, y) is represented by$Gray_{xy}$. The maximum filter coverage is indicated FC_{max}.

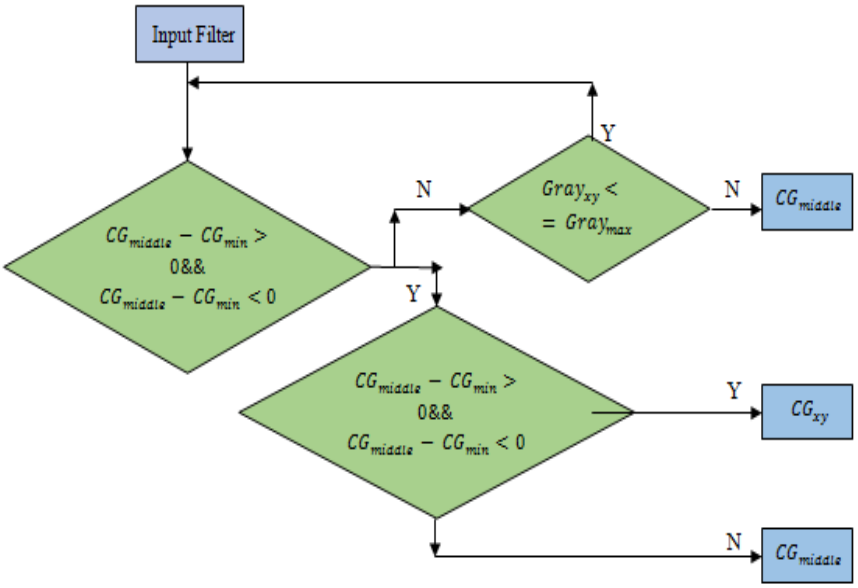

Figure 2: The Flowchart of AMF.

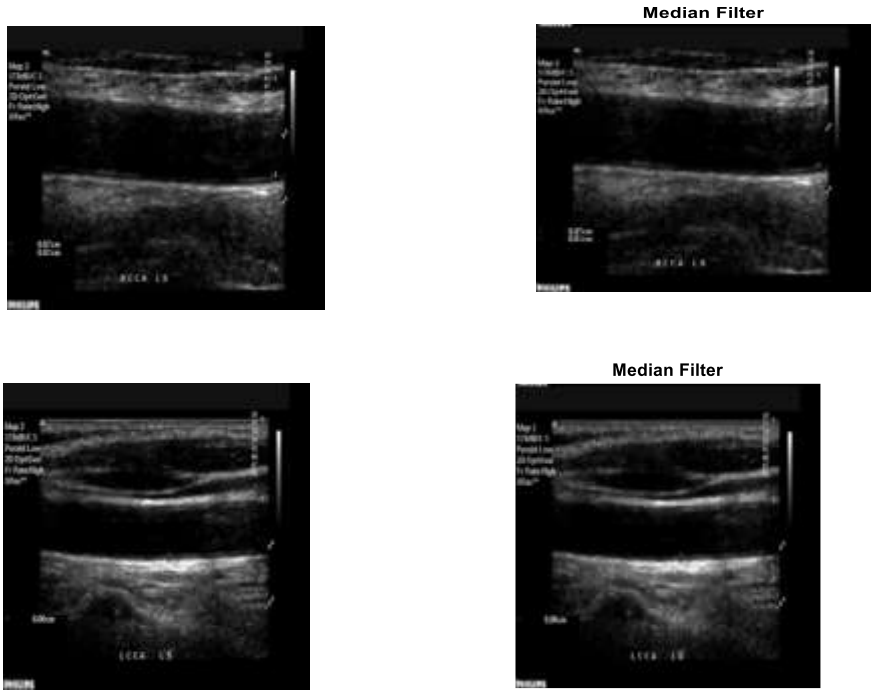

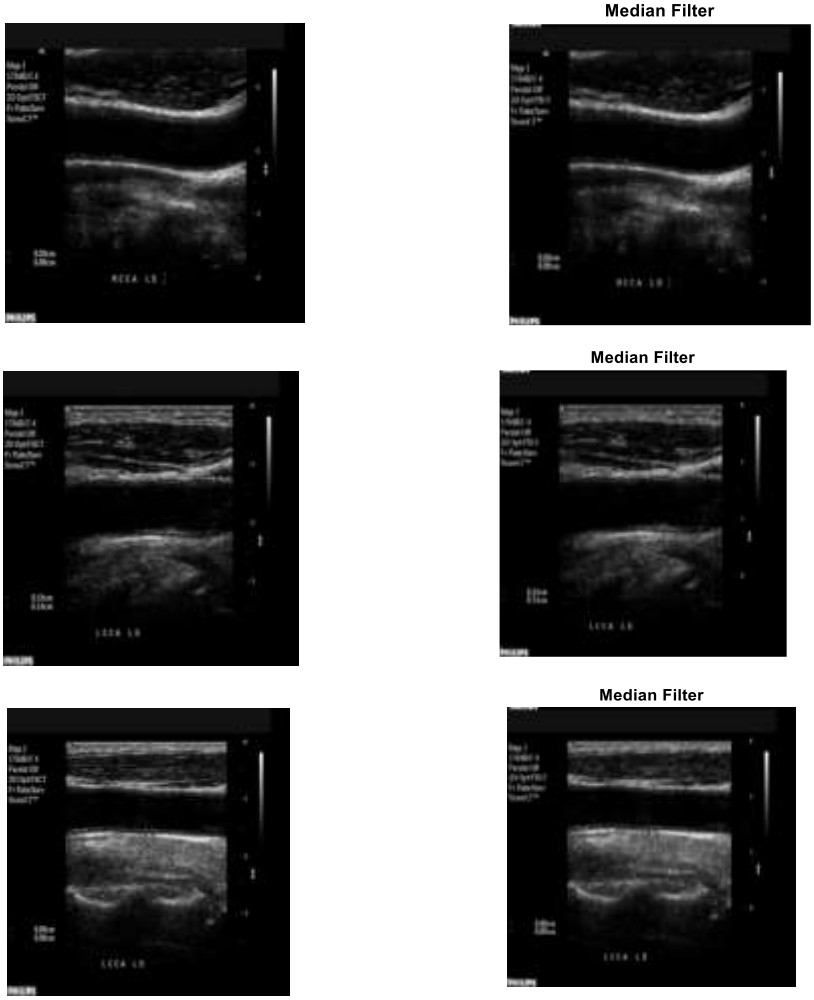

(a) Input Image *(b) Adaptive Median Filter*

Figure 3: The Results of AMF Filtering: (a) Input Image and (b) After Applying AMF.

4. DATA AUGMENTATION

Our dataset only had a small quantity of training data; thus we processed images using data augmentation methods. Data augmentation techniques have been shown to support a network's capacity for generalization and prevent overfitting. Training images may be artificially enhanced using random geometric alterations such as scaling, rotating, flipping, and moving, as demonstrated in Figure 4. This may also guarantee that the carotid plaque is the model's primary focus rather than other noise sources. The size of all up-scaled photos has been decreased to 256,256 pixels for uniformity.

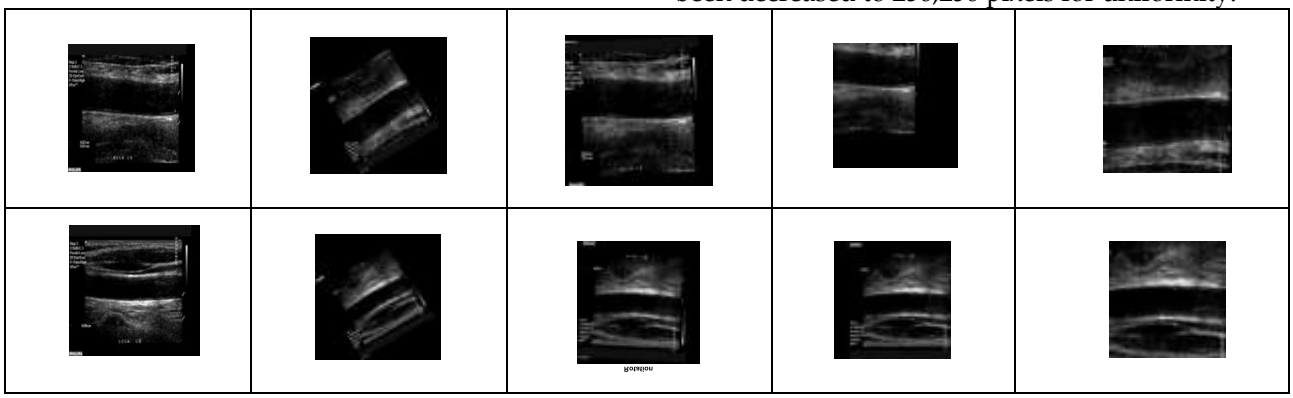

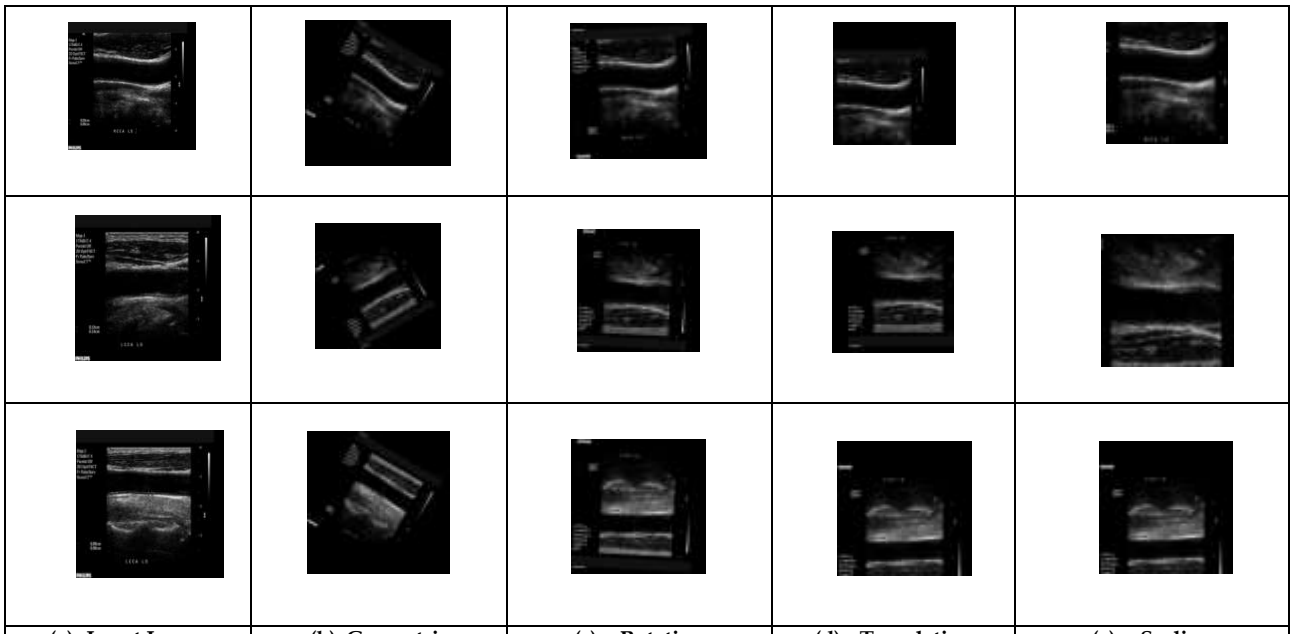

(a) Input Image	(b) Geometric Transformation	(c) Rotation	(d) Translation	(e) Scaling

Figure.4: The Results of Data Augmentation Process.

Proposed Segmentation Using SAC-U-Net When combined with U-Net, the examination mechanism has been described as an effective localization tool for screening that may be applied to medical images [16]. As a result, U-Net has been used in this study coupled with a scrutiny mechanism to enhance image segmentation performance.

Scrutiny mechanism: The convolution with increased scrutiny takes both the feature and spatial subspaces into account. They show that scrutiny augmentation improves US image categorization significantly. Irwan et al. [17] perform multihead scrutiny (MHA) on the flattening input matrix $\mathcal{X} \in \mathcal{R}^{\mathcal{H}\mathcal{W}} x \mathcal{F}_{in}$ in given an input stimulation map tensor of height $\mathcal{H}$, width $\mathcal{W}$, and channels $\mathcal{F}_{in}$,. The following formula is used to determine the single-head self-scrutiny ($S_{\hbar}$):

$$S_{\hbar} = softmax\left(\frac{(\mathcal{X}\mathcal{W}_q)(\mathcal{X}\mathcal{W}_{\hbar}^{\mathcal{T}})}{\sqrt{d_{\hbar}^{\hbar}}}\right)(\mathcal{X}\mathcal{W}_v) \qquad \textbf{(1)}$$

The linear transformations that transfer the stimulation chart characteristics to queries Q, keys K, and values V are $\mathcal{W}_q$, $\mathcal{W}_{\mathcal{K}} \in \mathcal{F}_{in} d_{\hbar}^{\hbar}$ and $\mathcal{W}_v \in \mathbb{R}\mathcal{F}_{in} \times d_{\hbar}^{\hbar}$. Concatenated multi-head outputs were subsequently contoured to correspond with the original $(\mathcal{H}, \mathcal{W}, d_v)$. dimension. To obtain the scrutiny-augmented convolution output, both convolution and scrutiny maps of features are combined in the final step [18].

The SAC-U-Net module is a crucial step in gaining deeper understanding of how scrutiny-augmented convolution modules are integrated into U-Nets in particular and segmentation contexts in general. It was discovered that networks used for image segmentations suffered when U-Net's convolution blocks were changed to enhanced supervision inversion blocks. The segmentation findings are encouraging since they intelligently collect just the most crucial and essential non-local contextual information by placing it at the U-Net bottleneck. With minimal change in model complexity, it has been demonstrated that the bottleneck test block enables the network to depend permanently on the lowest granularity of the activation map and yields noticeably better outcomes.

A number of different conventions for naming have been employed in this work, which are comparable to those of the annotations by Irwan et al. [17]: $\mathcal{H}, \mathcal{W}$ and Fin are abbreviations for the activation maps' height, width, and the number of input filters. In multi-head scrutiny, the terms $\mathcal{N}, \hbar, dv$ and d_k signify, respectively, the total number of heads, the depth of values, the depth of queries, with the depth of keys.

Self-scrutiny over (bottleneck) feature channel: The suggested U-Net approach is used to systematically process a source image (tensor) of configuration$(\mathcal{H}, \mathcal{W}, \mathcal{F}_{in})$,) for generating maps of features using standard convolution operators. The activation map is sampled using the maxpooling procedure. The reduced activation map, which has undergone the most recent down sampling processes in U-Net and has the lowest feature maps, is used to calculate the test maps.

According to Bello et al. [18], scan-enhanced convolution combines convolution characteristics with a scan feature map. The convolution feature maps generated and improved by scrutinising are gradually re-sampled through the sampling pipeline in combination with the convolution activation maps from the preceding down sampling layer. U-Net instance. More details on the U-Net architecture utilised in this work and the inclusion of augmented convolution in the test are provided in the sections that follow.

Proposed SAC-U-Net network architecture: The architecture of the model includes scrutiny-augmented convolution network [17] and U-Net [18] principles. This suggested innovation network makes use of Supervision Enhancement Structures in the context of the Enhancement framework monitor to leverage the qualities of the Supervision Enhancement framework to comprehend the whole viewpoint and capture long-term dependencies. The block diagram for the SAC-U-Net, or proposed supplemental check U-Net, is shown in Figure 5.

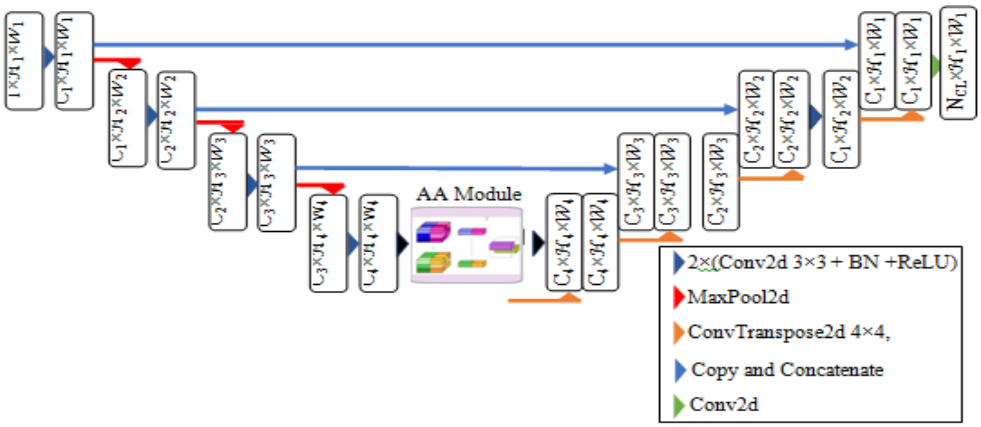

Figure 5: The Architecture Diagram of SAC-U-Net.

To best analyze the 256256 image dimension of interest, a U-Net architecture structure [19, 20] is being used, with a modest adaptation made by lowering one down sampling (and matching up sampling channel). The down sampling path has three blocks, while the upsampling block has three blocks. Batch normalization, 2D convolution (kernel sizes:33; strides:1) and ReLU are the three elements that make up each block. The last block [23] is a two-dimensional convolution block with size 11 kernels. By using max pooling in the down sampling step, the geographic size of the feature map is halved after each block. The enhanced sampling route uses ConvTranspose2d to increase the spatial size of the concatenated feature map by two. The total number of channels for the features is increased by 1-64-128-256-512 during down sampling and correctly decreased again during resampling. The final layer of the U-Net produces a set of feature channels with a set of label categories for image segmentation.

The test-augmented convolution module uses the neighbourhood representation feature maps produced by final U-Net blocks during down sampling phases as information for reducing dimensionalities. The evaluation augmentation convolution module is added into the bottleneck, helping decrease computing costs due to the smaller size of the feature map and the lower and more manageable spatial and temporal complexity of the evaluation map. The first test-augmented convolutional network built using the ResNet architecture was implemented [18] [21]. Scrutiny augmentation was added to each of these remaining layers in the last three phases of the ResNet architecture. Whenever the dimension of space of the activation-argument combination is problematic for large spatial dimensions $\mathcal{O}((\mathcal{H}\mathcal{W})^2\mathcal{N}_h)$)scrutiny-augmented convolution was used in the original work.

Scrutiny augmented convolutions are determined on third and final down-sampling blocks of U-Nets in the proposed SAC-U-Net on activation maps (Fig. 5). During the level, there are 128 activation channels, and the image is 32 by 32 pixels in size. In the current integration realization, three scrutiny heads, four scrutiny heads, four depths of values (d_v), and forty depths of queries and keys (d_v) have been employed for the scrutinizing-augmented convolution kernel. The next step is to combine the generated investigation activation feature maps with the ordinary convolution scrutiny maps from the previous down sampling block. The up-sampling path of the U-Net is then traversed using the concatenated scrutiny maps.

When contrasted with the background class, the infectious agent class during CCA image data is typically underrepresented, especially in the initial phases of the disease. This causes a serious issue of class inequality. Studies have shown that ground-glass opacities typically come before consolidation plaques. This development of the plaque in the CCA image proceeds to another instance of class inequality. Only one of the plaques may be significantly present in some patients, while the second one may only account for less than 10% of all infection labelling. This results in a second type of class inequality. The opposite direction class-weighted loss of cross-entropy has been suggested as a solution to all the aforementioned class-imbalance problems, which are particularly prevalent in CCA imaging plaque segmentation contexts. Inversely proportionate to the square of the power of class frequency is how the weights are calculated. This inverted category-weighted loss of cross-entropy can be written as follows for a sample with the class label y:

$$\mathcal{CE}(z, y) = w_y \left(-\log \left(\frac{exp(z_y)}{\sum_{j=1}^{\mathcal{C}} exp(z_j)} \right) \right) \quad (2)$$

$\mathcal{C}$ is the overall number of classes, and $\mathcal{Z}$ is the model's output for all classes. The weighing element

$$w_y = \frac{\sqrt{\frac{1}{z_y}}}{\frac{1}{\mathcal{C}} \sum_{j=1}^{\mathcal{C}} \sqrt{\frac{1}{z_y}}} \quad (3)$$

w_y is derived using inverses of square roots of total occurrences in label classes to address imbalances in training data. Due to heterogeneous distributions of the sets used for training and validations, the inverse weights of sets are determined separately. The best learning speeds and potentially maximum degree of learning are determined using higher education policy planners and learning rate finders. The input image, segmentation, and output of image processing are displayed in Figure 6.

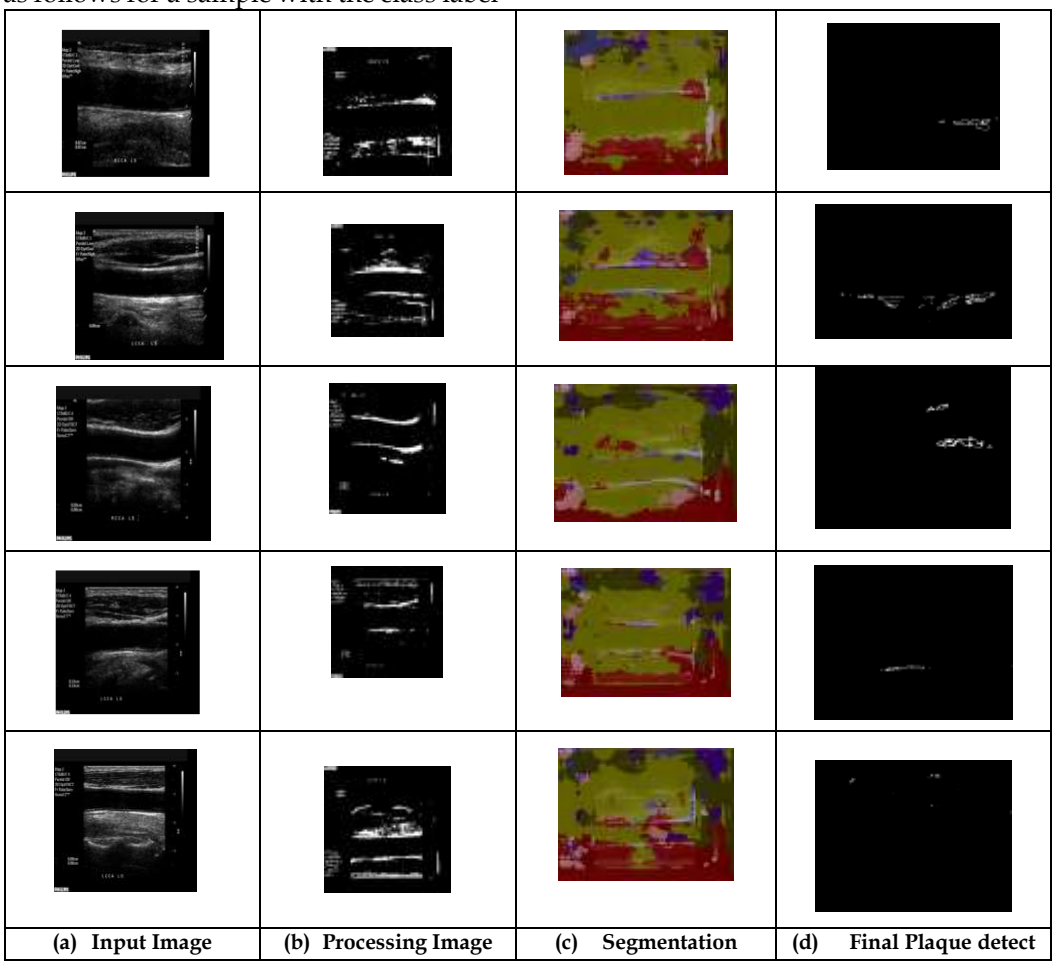

Figure 6: The Process of Input Image, Segmentation, and Output of the CP Detection Images.

5. EXPERIMENTAL RESULTS AND DISCUSSION

Recent studies have demonstrated that, in comparison to employing a single modality, the discriminative performance tends to be better by taking into account all of the characteristics from

several modalities. Because these two produce rich and varied intensities within the data, SAC- U- Net model-based radiomic approaches were therefore developed in the current work for learning from datasets. The confusion matrix, which summarizes the classification efficacy of a machine learning algorithm based on the evaluation dataset, was calculated in this work. Dice Similarities Coefficient (DSC), precision, accuracy, and sensitivity are compared to existing approaches like U-Net, Dilated U-Net, and Improved U-Net as well as the proposed SAC-U-Net. In this instance, the parameter known as the dice similarity coefficient (DSC), which is generated using the equation shown below, is utilized to estimate the precise ratio between the accessible real or plaque and accessible plague or non-plague pixels to the predicted pixels.

$$\mathrm{DSC} = \frac{(2\mathrm{TP})}{(\mathrm{FP}+2\mathrm{TP}+\mathrm{FN})} \times 100 \qquad (4)$$

The non-plaque mass classified as Non-Plaque (True Negative) is the first; the non-plaque mass categorized as Plaque (False Positive) is the second; the Plaque mass classified as Plaque (TP) is the third; and the Plaque masses classified as Non-Plaque (FN) is the fourth. The confusion matrix, one of the important metrics used to assess classification accuracy, is made up mostly of these four variables. Additionally, the following calculations were made using the True Negative (TN) and True Positive (TP) measurements:

$$Precision = \frac{TP}{TP + FP} \qquad (5)$$

$$Recall = \frac{TP}{TP + FN} \qquad (6)$$

$$Overallaccuracy = \frac{TP + TN}{TP + FN + TN + FP} \qquad (7)$$

In addition to the quantitative measurements, accuracy/loss graphical representations over the total number of epochs are used to qualitatively assess network performance. The loss of testing, validation, and training data was measured during the training period, as shown in Fig. 7. The proposed model's accuracy was 99.85%, and its error was 0.1.

Figure 7: Training and Validation Loss against the Number of Epochs for the Proposed Method.

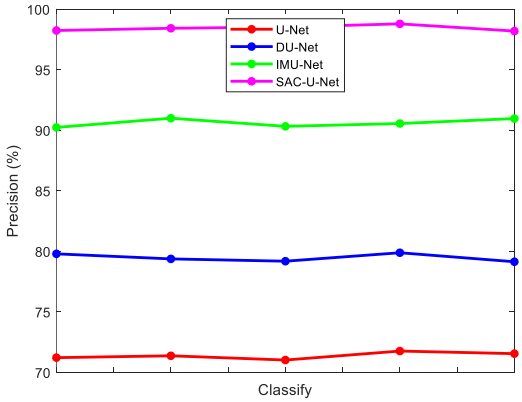

Figure 8: Precision Comparison Results between the Proposed and Existing Methods for Segmenting the Carotid Plaque Data.

The precision comparison between the proposed and current methods for categorizing the Carotid Plaque data is shown in Fig. 8. According to the findings, the suggested Enhanced U Net Models and SAC-U-Net approach produce results with a higher degree of precision than those produced by the

currently used classification methods. The accuracies of suggested and current models for characteristics in particular databases are shown in Figure. The SAC-U-Net that has been suggested improves accuracy by 98.844%. The effectiveness of the suggested approach SAC-U-Net differs from the U-Net, Dilated U-Net, and Improved U-Net in two key ways. One is that the regular U-Net, Dilated U-Net, and Improved U-Net advantages are all combined in the suggested deep model. The categorization effect of U-Net may be greatly enhanced by this SAC-U-Net, which also caused it to narrow down to a reduced loss value during training

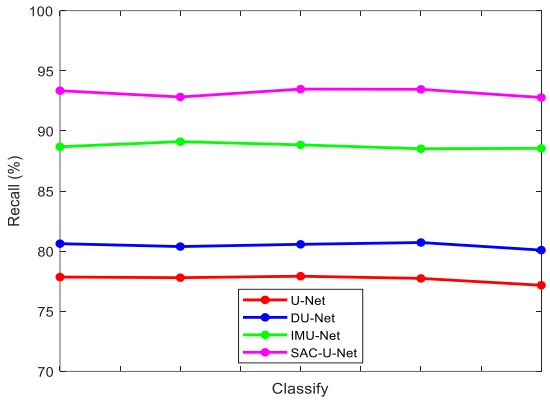

Figure 9: Recall Comparison Results Between the Proposed and Existing Methods for Segmenting the Carotid Plaque Data.

Figure 9 displays the recall comparison of the proposed and existing approaches for categorising carotid plaque data. The results show that the enhanced U Net model and the SAC-U Model. In comparison to existing categorization techniques, the suggested -Net and SAC-U-Net approaches perform well in terms of recall. The suggested SAC-U-Net model, which has been trained to recognise impacted areas in ultrasound pictures, has demonstrated repeatable findings that may be used as a true smart device in medical imaging. Other research has looked into the potential of DL-based models to distinguish between illnesses from various historical eras. The figure compares U-Net, dilated U-Net, and improved U-Net.There are numerous DL models that are used to identify, categorize, and explain leaf disease in plants. SAC-U-Net achieves 94.867% on US images. Additionally, compared to other approaches for segmentation, the SAC-U-Net methodology is a quick method with less computational complexity.

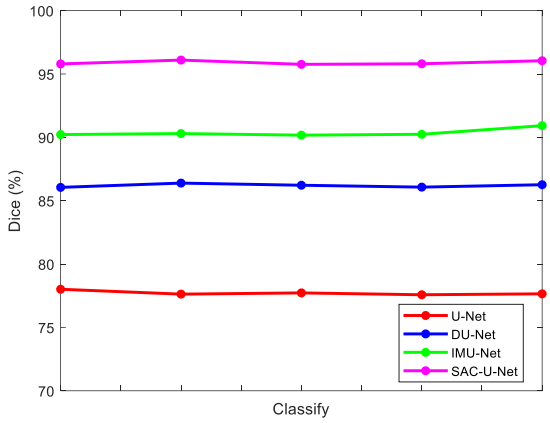

Figure 10: Dice Coefficient Comparison Results between the Proposed and Existing Methods for Segmenting the Carotid Plaque Data.

The Dice Coefficient comparisons between the proposed and current methods for categorizing the Carotid Plaque data are shown in Fig. 10. According to the findings, the suggested Enhanced U Net Model and SAC-U-Net methodology outperform existing classification methods by a significant margin. The specificity of suggested and current models for the quantity of features in a particular database is shown in Fig. 10. Recall is maximized as the quantity of features increases. Comparing the SAC-U-Net with the Normal U-Net, Dilated U-Net, and Improved U-Net yields a recall of 96.814%. Existing approaches are underfitting because they use basic models that are inefficient for high-dimensional datasets. It is clear that the suggested SAC-U-Net algorithm's stability and universality are strong in addition to its excellent segmentation accuracy.

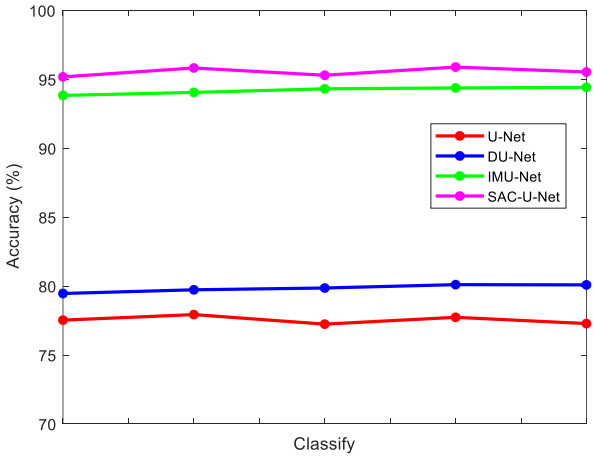

Figure 11: Accuracy Comparison Results between the Proposed and Existing Methods for Segmenting the Carotid Plaque Data.

The accuracy comparison among the proposed and current methods for categorizing the Carotid

plaque data is shown in Fig. 11. The upgraded U Net model and the SAC-U-Net approach are shown to be more accurate than the segmentation techniques currently in use. SAC-U-Net's accuracy rises to 97.001% and the sensitivity is attained when compared to U-Net, Relaxed U-Net, Enhanced U-Net, and SAC-U-Net. Therefore, in terms of accurate cancer prediction validation findings, the suggested technique performs better than existing algorithms. Additionally, we see that CNN converges later than other techniques. As a result, SAC-U-Net's deep structure frequently takes a while, especially when there is a lot of input. The deep structure of this network, as opposed to other networks, is the main factor in its greater recognition rate.

6. CONCLUSION AND FUTURE WORK

The U-Net module has been given a fresh adaptation with scrutiny augmentation in this work. The differentiation of plaque areas in US images is improved by this SAC-U-Net. The creative approach and astute mix of scrutinizing augmentation in the U-Net bottleneck has proven to be a successful combination producing excellent and encouraging results. Cutting-edge infection segmentation models, have enormous potential to help clinicians more effectively. SAC-U-Net performs almost as well as upgraded U-Net while outperforming Criss-Cross-Attention (CCA). The inclusion of attention augmentation in further U-Net phases will be investigated in subsequent investigations. Another possible study area to look into is deforming scrutiny augmentation. There are additional scrutiny augmentation factors that can significantly affect segmentation performance while also sharply increasing the number of parameters that are trainable thereby increasing the GPU requirements. Examples of these parameters are the total amount of scrutiny heads and channels. To develop better configurations of using scrutiny augmentation more successfully, more studies will be done here. The supplemental materials have recorded the infection-related localization efficacy of SAC-U-Net on each patient, the multi-label segmented performance of SAC-U-Net on each patient, and a mean of multilabel localization performance across the patients. The average segmentation performance for the proposed SAC-U-Net across all patients gives an impressive Dice score of 96.814. In comparison to baseline U-Net models or state-of-the-art models, the suggested scrutiny-augmented U-Net is significantly more capable of segmenting and consolidating plaques.

REFERENCES

[1] Asadullah, K. S., Mahar, S., Faham, M., Hameed, M., & Zafar, H. (2022). Sensitivity and Specificity of Color Duplex Ultrasound Measurement in the Estimation of Internal Carotid Artery Stenosis. *Pakistan Journal of Medical & Health Sciences, 16*(11), 821-821.

[2] Saba, L., Saam, T., Jäger, H. R., Yuan, C., Hatsukami, T. S., Saloner, D., ... & Wintermark, M. (2019). Imaging biomarkers of vulnerable carotid plaques for stroke risk prediction and their potential clinical implications. *The Lancet Neurology, 18*(6), 559-572.

[3] Weng, S. T., Lai, Q. L., Cai, M. T., Wang, J. J., Zhuang, L. Y., Cheng, L., ... & Qiao, S. (2022). Detecting vulnerable carotid plaque and its component characteristics: Progress in related imaging techniques. *Frontiers in Neurology, 13*, 982147.

[4] Jain, P. K., Sharma, N., Saba, L., Paraskevas, K. I., Kalra, M. K., Johri, A., ... & Suri, J. S. (2021). Unseen artificial intelligence—Deep learning paradigm for segmentation of low atherosclerotic plaque in carotid ultrasound: A multicenter cardiovascular study. *Diagnostics, 11*(12), 2257.

[5] Zhou, R., Azarpazhooh, M. R., Spence, J. D., Hashemi, S., Ma, W., Cheng, X., ... & Fenster, A. (2021). Deep learning-based carotid plaque segmentation from B-mode ultrasound images. *Ultrasound in Medicine & Biology, 47*(9), 2723-2733.

[6] Akkus, Z., Carvalho, D. D., van den Oord, S. C., Schinkel, A. F., Niessen, W. J., de Jong, N., ... & Bosch, J. G. (2015). Fully automated carotid plaque segmentation in combined contrast-enhanced and B-mode ultrasound. *Ultrasound in Medicine & Biology, 41*(2), 517-531.

[7] Qian, C., & Yang, X. (2018). An integrated method for atherosclerotic carotid plaque segmentation in ultrasound image. *Computer Methods and Programs in Biomedicine, 153*, 19-32.

[8] Cheng, J., Chen, Y., Yu, Y., & Chiu, B. (2018). Carotid plaque segmentation from three-dimensional ultrasound images by direct three-dimensional sparse field level-set optimization. *Computers in Biology and Medicine, 94*, 27-40.

[9] Loizou, C. P., Pattichis, C. S., Istepanian, R. S. H., Pantziaris, M., & Nicolaides, A. (2004, September). Atherosclerotic carotid plaque segmentation. In *The 26th Annual International Conference of the IEEE Engineering in Medicine and Biology Society* (Vol. 1, pp. 1403-1406). IEEE.

[10] Akkus, Z., De Jong, N., Van Der Steen, A. F., Bosch, J. G., Van Den Oord, S. C., Schinkel, A. F., ... & Klein, S. (2014, September). Fully automated carotid plaque segmentation in combined b-mode and contrast enhanced ultrasound. In *2014 IEEE International Ultrasonics Symposium* (pp. 911-914). IEEE.

[11] Loizou, C. P., Petroudi, S., Pantziaris, M., Nicolaides, A. N., & Pattichis, C. S. (2014). An integrated system for the segmentation of atherosclerotic carotid plaque ultrasound video. *IEEE Transactions on Ultrasonics, Ferroelectrics, and Frequency Control, 61*(1), 86-101.

[12] Galluzzo, F., Corsi, C., Morizzo, C., De Marchi, L., Testoni, N., Speciale, N., & Masetti, G. (2014, September). Capsu: A completely automated method for carotid plaques segmentation in ultrasound images. In *Computing in Cardiology 2014* (pp. 309-312). IEEE.

[13] Galluzzo, F., De Marchi, L., Testoni, N., Tabassian, M., Speciale, N., & Masetti, G. (2014, September). A fully automated method for carotid plaques segmentation in ultrasound images based on motion estimation and level-set. In *2014 IEEE International Ultrasonics Symposium* (pp. 2343-2346). IEEE.

[14] Loizou, C. P., Petroudi, S., Pantziaris, M., Nicolaides, A. N., & Pattichis, C. S. (2014). An integrated system for the segmentation of atherosclerotic carotid plaque ultrasound video. *IEEE Transactions on Ultrasonics, Ferroelectrics, and Frequency Control, 61*(1), 86-101.

[15] Van Engelen, A., Van Dijk, A. C., Truijman, M. T., Van't Klooster, R., Van Opbroek, A., van der Lugt, A., ... & de Bruijne, M. (2014). Multi-center MRI carotid plaque component segmentation using feature normalization and transfer learning. *IEEE Transactions on Medical Imaging, 34*(6), 1294-1305.

[16] Ibtehaz, N., & Rahman, M. S. (2020). MultiResUNet: Rethinking the U-Net architecture for multimodal biomedical image segmentation. *Neural Networks, 121*, 74-87.

[17] B, Irwan, Barret Zoph, Ashish Vaswani, Jonathon Shlens, and Quoc V. Le. (2019). "Attention augmented convolutional networks." In *Proceedings of the IEEE/CVF International Conference on Computer Vision*, pp. 3286-3295.

[18] Ronneberger, O., Fischer, P., Brox, T. (2015). U-net: Convolutional networks for biomedical image segmentation. In *International Conference on Medical Image Computing MICCAI*.

[19] MedicalSegmentation.com. CCA image CT segmentation dataset. http://medicalsegmentation.com/covid19/

[20] Schlemper, J., Oktay, O., Schaap, M., Heinrich, M., Kainz, B., Glocker, B., Rueckert, D. (2019). Attention gated networks: Learning to leverage salient regions in medical images. *Medical Image Analysis, 53*, 197–207.

[21] Vaswani, A., Shazeer, N., Parmar, N. U., Jakob, J., Llion, G., Aidan, Kaiser, N., Polosukhin, I. (2017). Attention is all you need. In *Proceedings of the 31st International Conference on Neural Information Processing Systems*.

[22] P. Jonnala and G. S. Reddy. (2023). "Image de-noising of Ultrasound Carotid artery images using various filters," *2023 4th International Conference for Emerging Technology (INCET)*, Belgaum, India, pp. 1-4, doi: 10.1109/INCET57972.2023.10170198.

[23] Kothala, L. P., Jonnala, P., & Guntur, S. R. (2023). Localization of mixed intracranial hemorrhages by using a ghost convolution-based YOLO network. *Biomedical Signal Processing and Control, 80*, 104378.